17

Monte Carlo Modeling of Light Propagation in Neonatal Skin

J.A. Delgado Atencio[1], S.L. Jacques[2] and S. Vázquez y Montiel[1]
[1]*Instituto Nacional de Astrofísica Óptica y Electrónica,*
[2]*Oregon Health & Science University-Dermatology/Biomedical Engineering,*
[1]*México*
[2]*USA*

1. Introduction

The origin of the "Monte Carlo method" historically comes from Los Alamos National Laboratory in the early years after the Second World War and is related with two important events that took place in 1945: the successful test at Alamogordo and the building of the first electronic computer (the ENIAC) (Metropolis, 1987). After the review of the ENIAC results held in the spring of 1946 at Los Alamos, Stanislaw Ulam realized that statistical techniques in combination with the surprising speed and the versatility of this electronic computer could lead to a powerful tool in theoretical calculations (Metropolis, 1987). On March 11, 1947, John von Neumann in a handwritten letter included a detailed outline of a possible statistical approach (incorporating Stanislaw´s idea) to solving the problem of neutron diffusion in a spherical core of fissionable material surrounded by a shell of tamper material. At that time, Nick Metropolis suggested the name "Monte Carlo" for the re-emerging sampling technique (Metropolis, 1987).
However, a previous work performed by Enrico Fermic in neutron diffusion in Rome in the early thirties, incorporated the essential principles of the Monte Carlo method when he was studying the moderation of neutrons (Metropolis, 1987). Another example of the previous use of this sampling technique is an ancient problem in geometric probability: "The Buffon's needle problem" which was stated in 1733 and solved (solution published in 1777) by Geroges Louis Leclerc, Comte de Buffon (1707-1788) (Weisstein, accessed September 2010). In this problem the probability of the needle crossing a line (in a table marked with equidistant parallel lines) is proportional to the inverse of the number π provided that the length of the needle is less than the space between lines. The repetition of this experiment many times results into the assessment of π.
During the post-war period the Monte Carlo (MC) method spread into many fields of knowledge such as astrophysics, solid state, optics, etc. One example in astrophysics is the study of the transfer of visible radiation through terrestrial clouds using a MC computer program that incorporated the Henyey-Greenstein phase function to describe the scattering process of water droplet clouds (Danielson et al., 1969). Another illustration of this method appears in the book "The Monte Carlo Methods in Atmospheric Optics" (Marchuk et al., 1980) which had a first Russian edition in 1974. In the preface of this book an acceptable definition of the MC method is given which is reproduced here:

"The most universal method for solving the above mentioned problems is the Monte Carlo method, which is a numerical simulation of the radiative-transfer process. This process can be regarded as a Markov chain of photon collisions in a medium, which result in scattering or absorption. The Monte Carlo technique consists in computational simulation of that chain and in constructing statistical estimates of the desired functionals".

In 1983 the MC method was applied for the first time to determine light distribution in biological tissues (Wilson & Adam, 1983), and it was specially designed to predict the distribution of absorbed dose in homogeneous tissues irradiated either by external beam light or by mean of interstitial optical fibers. After this pioneer work, various MC approaches to deal with light propagation in turbid media has been developed and applied to specific problems in the field of biomedical optics (Hasegawa et al., 1991; Graff et al., 1993; Wang et al., 1995; Wang et al., 1997). Currently, new improvements regarding the reduction of the intrinsic high computation time of Monte Carlo codes have been performed (Alerstam et al., 2008; Lo et al., 2009) by either an FPGA (field-programmable gate arrays) or GPU (graphics processing units) based platform. The significance of the results obtained so far is that this new platform may potentially enable real-time treatment planning in interstitial Photodynamic Therapy (PDT). It is interesting to observe that the same application (interstitial photodynamic therapy (PDT)) in which the MC method was applied for the first time to light distribution in tissues in 1983, is nowadays one of the most outstanding field of continuous development in biomedical optics.

The application that this chapter presents is based on the use of the so-called Monte Carlo code MCML (Wang et al., 1995) to simulate the light propagation in neonatal skin affected with different grades of hyperbilirubinemia. The neonatal jaundice (hyperbilirubinemia) can have its origin in the accumulation of the bilirubin in the serum of the blood since the liver not yet has developed totally enzymes to oxidize the bilirubin. Hyperbilirubinemia (total level of serum bilirubin TSB>1.0 mg/dL) appears in almost all newborns, whereas significant hyperbilirubinemia (TSB > 12.9 mg/dL) and excessive hyperbilirubinemia appear in only 5 to 6% of the healthy population of newborns (Bhutani et al., 2000). An excessive level of bilirubin in neonates blood (29.2 mg/dL < TSB < 47.5 mg/dL) can induce changes in the mitochondria of the basal ganglia resulting in alterations of cerebral metabolism and producing permanent damage (Groenendaal et al., 2004). The subcommittee of hyperbilirubinemia of the American Academic of Pediatry (AAP) elaborated a clinical practical guideline for the management of hyperbilirubinemia in the newborn infant (Maisels et al., 2004). The third key element of the recommendations provided by this guideline states that clinicians should measure the total serum bilirubin (TSB) or transcutaneous bilirubin (TcB) level on infants jaundiced in the first 24 hours. Transcutaneous bilirubin levels have been measured non-invasively, for instance with the transcutaneous device BiliCheck (Respironics, Marietta, GA) in a multicenter evaluation study (Rubaltelli et al., 2001) and with the transcutaneous jaundice meter model JM-103 (Minolta) in a multiracial population study of 849 newborns **>35** weeks of gestation (Maisels et al., 2004). One remarkable conclusion in this multicenter study is that BiliCheck can be used as a reliable substitute of TSB assessment whereas the JM-103 bilirubinometer correlates well with TSB levels for the entire population with the exception of black newborn infants where TcB levels are rather overestimated (Maisels et al., 2004). Two classical papers (Jacques et al., 1997, Delcher, et al. accessed April, 2007) contain the working principles of BiliCheck, presenting the basics underlying development of an optical fiber spectrometer for measurement of TcB levels in newborn infants. The working principle of

this measurement accounts for variations in dermal scattering, melanin content and cutaneous blood content by using the spectrum of visible light 380-760 nm for a total of 221 spectral points (Kolman et al., 2007).
This chapter reports on the use of Monte Carlo modeling to numerically simulate the diffuse reflectance spectrum of neonatal skin in the spectral region 400-700 nm. The Monte Carlo code MCML (Wang et al., 1995) can accurately consider the multiple layers of a complex structure like the skin which is modeled in this study as a three layer optical medium: epidermis, dermis and subcutaneous tissue. In order to implement the spectral simulation of diffuse reflectance, two codes in Matlab were developed to facilitate this task. Simulation results considering the influence of factors such as: bilirubin content, grade of epidermis pigmentation, content of blood and slight variation of refractive index of skull and subcutaneous layer are presented. The significance of this study is that from MC simulations in a wide spectral region is deduced the potential possibility of using the narrow spectrum of visible light from LEDs to design and develop a low cost bilirubin meter for clinical applications in developing countries.

2. Materials and methods

2.1 Programming codes

The MC program MCML is written in standard C for modeling of the photon transport in multi-layered media, where the optical properties (μ_a, μ_s, g, n) and thickness (d) of each layer are known parameters (Wang et al., 1995). This simulation code describes the transport of an infinitely narrow photon beam perpendicularly incident on the multi-layered medium. The response of a multi-layered tissue system, speaking in terms of the simulated quantities, due to this interaction is called the impulse response or Green's function (Wang & Jacques, 1992-1998). The reflectance, transmittance, photon absorption and fluence, are the physical quantities simulated with this code. The MCML simulation records the escape of photons at the top Rd(r, α) and bottom Tt(r, α) surfaces of a multi-layered tissue slab as local radial reflectance and transmittance, respectively. Here α is the angle between the photon exiting direction and the normal to the tissue surfaces. In this work, we are only interested in simulating the total diffuse reflectance R_d of neonatal skin since this physical quantity or a fraction of it can be easily measured in-vivo.
One important feature of simulating with MCML code is the possibility to prepare a single input data file for multiple and independent runs where the number of runs is not limited by the memory capacity of the computer. We took advantage of this distinct property to naturally implement the spectral simulation of diffuse reflectance R_d (λ_i) by linking optical properties (μ_a, μ_s, g, n) at a discrete wavelength λ_i with the ith independent run. Therefore, there will be as many independent runs in the input data file as discrete wavelengths in the spectral region of interest. Another distinguishing characteristic of this software is that for each independent run defined in the input file there will be only one output data file which will contain all the above mentioned simulated quantities. So, the code will generate as many output file as discrete wavelengths of interest have been defined by the user.
Based on the main features described in previous paragraphs, the code MCML was combined with two programs in Matlab developed by us in order to facilitate the task of spectral simulations over a relatively wide spectral range (400-700 nm) with 31 spectral points and 10 nm of increment. The first Matlab program is called MCinput (see Appendix 1) and is used to prepare the input data file with extension .mci for multiple runs of the MCML

program. In this case each run corresponds to optical and geometrical parameters given at a specific wavelength as stated above. The second program is called MCoutput (see Appendix 1) and is used to read the recorded total diffuse reflectance Rd from the multiple output data files with extension .mco corresponding to each wavelength of the spectral range.
A total of $5x10^4$ photons were launched for each specified wavelength in order to simulate the diffuse reflectance with the adequate precision. This number of launched photons is more than one order of magnitude higher than the required typical number of photons (3000) for modelling the total diffuse reflectance from a turbid medium of specified optical properties (Wang & Jacques, 1992-1998).

2.2 Optical model of neonatal skin

The model mimics the body site were TcB measurements are performed in clinical applications: the forehead. In this site we considered the skin formed by three flat and infinite layers that lie on the frontal bone of the infant being the air and skull the top medium and the bottom medium, respectively as it is shown in figure 1.

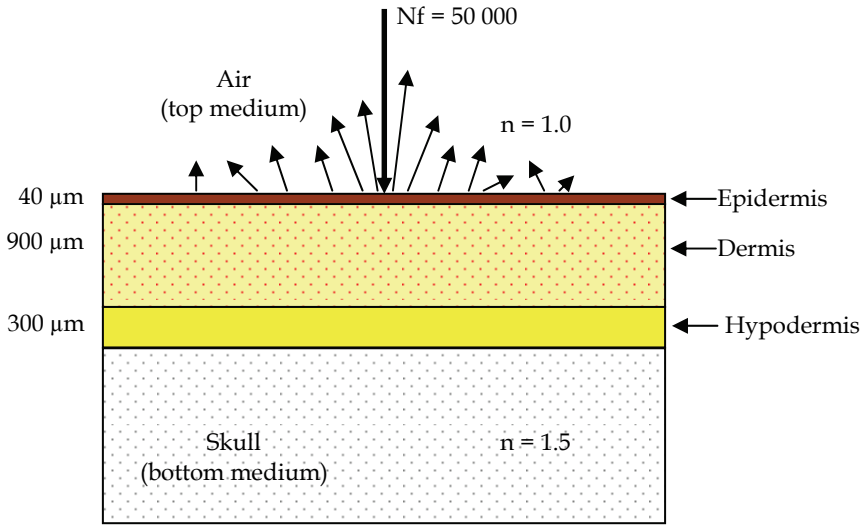

Fig. 1. Schematic representation of the tree-layer skin model of the forehead of newborn infants. The skin is considered as a 3-D half-infinite medium divided into three layers: epidermis, dermis and subcutaneous tissue (or hypodermis). The top medium is the air surrounding epidermis and the bottom medium is the skull.

The most external layer is epidermis where melanin is the only absorber and is considered as being uniformly distributed in epidermis thickness of about 40 µm. The volume fraction of melanosomes in this layer is denoted by f_{me} and its absorption coefficient is calculated as:

$$\mu_{a\_epidermis}(\lambda) = f_{me}\mu_{a\_me}(\lambda) \tag{1}$$

here $\mu_{a\_me}(\lambda) = 6.6 \times 10^{11} \lambda^{-3.33}$ is an approximate analytical expression for the absorption coefficient of the interior of a melanosome (Jacques, 1998).

The second layer, from the surface to the depth, is the dermis. We considered in this layer two primary absorbers, the blood and the bilirubin, which are both assumed to uniformly distribute in the dermis (900 μm). The volume fraction of blood vessels containing whole blood is denoted by f_{bl}. Collagen fibers are considered as the only elements to determine the scattering coefficient in epidermis and dermis. Scattering coefficient is considered the same for both epidermis and dermis (Jacques, 1998). Bilirubin concentration in the blood, C_{bi} [g/L], the extinction coefficient $\varepsilon_{bi}(\lambda)$ [cm^{-1}/(moles/L)] and the gram molecular weight P_{Mbi} [g/moles] of bilirubin molecule are put together into equation (2) with a numerical factor, ln(10), such that absorption coefficient due to bilirubin was

$$\mu_{a\_bi}(\lambda)=\ln(10)\frac{C_{bi}}{P_{Mbi}}\varepsilon_{bi}(\lambda) \tag{2}$$

Then equation (2) was scaled by a fixed partition coefficient f_{bi} (kept constant at 0.20, in reality, should vary nonlinearly as C_{bi} exceeds holding capacity of serum albumin), to account for the fact that bilirubin enters the dermis at a fraction of its concentration, C_{bi}, in blood vessels. The volume fraction of whole blood in skin is f_{bl}, which scales the absorption coefficient of whole blood, μ_{a_blood}, based on 150 g haemoglobin per liter blood. Hence, the total dermis absorption is:

$$\mu_{a\_dermis}(\lambda) = f_{bl}\mu_{a\_blood} + f_{bi}\mu_{a\_bi}(\lambda) \tag{3}$$

The first and second terms in equation (3) are the average absorption coefficient of the dermis due to blood and bilirubin, respectively. In turn, the absorption coefficient of blood, μ_{a_blood} , is calculated as

$$\mu_{a\_blood}(\lambda) = S\mu_{a\_oxy} + (1-S)\mu_{a\_deoxy} \tag{4}$$

here S is the oxygen saturation of blood and μ_{a_oxy} and μ_{a_deoxy} are the absorption coefficients of oxy-hemoglobin (HbO_2) and deoxy-hemoglobin (Hb), respectively. A similar expression to equation (2) is used for these coefficients:

$$\mu_{a\_oxy}(\lambda) = \ln(10)\frac{C_{bl}}{P_{Mbl}}\varepsilon_{oxy}(\lambda),\ \mu_{a\_deoxy}(\lambda)=\ln(10)\frac{C_{bl}}{P_{Mbl}}\varepsilon_{deoxy}(\lambda) \tag{5}$$

Extinction coefficient for bilirubin $\varepsilon_{bi}(\lambda)$, oxy-hemoglobin $\varepsilon_{oxy}(\lambda)$ and deoxy-hemoglobin $\varepsilon_{deoxy}(\lambda)$ used in dermis layer were taken from tabulated data published by Dr. Prahl (Prahl, accessed September 2010). The wavelength dependence of the anisotropy factor, g, was adopted from published optical properties (van Gemert et al., 1989) for epidermis and dermis of neonatal skin:

$$g(\lambda) = 0.62 + 0.29 * 10^{-3}\lambda \tag{6}$$

where the wavelength, λ , is in nanometres. This linear relationship yields values of g in the range 0.736-0.823 for the spectral region 400-700 nm used in this study.

The third layer included in the model is the subcutaneous tissue which is considered as a highly scattering and low absorption layer with a thickness of 300 μm. The absorption coefficient and the anisotropy factor were set as constant along the entire wavelength range with a value of 600 cm^{-1} and 0.8, respectively following published data (Tsumura et al.,

accessed January, 2006). The reduced scattering coefficient for epidermis and dermis was considered the same and was calculated following the expression reported in a published PhD thesis for a gestational age of 39 weeks (Randeberg, 2005) :

$$\mu_s'(\lambda) = C_{Mie}(1 - 1.745 * 10^{-3}\lambda + 9.844 * 10^{-7}\lambda^2) + C_{Rayleigh}\lambda^{-4} \quad (7)$$

where $C_{Mie} = 6800$ [m^{-1}], and $C_{Rayleigh} = 9.5 * 10^{13}$ [nm^4/m] are the Mie and Rayleigh constants, respectively and the wavelength is given in [nm].

2.3 Simulations

The first simulation focused on the dependence of the diffuse reflectance spectrum on the serum levels (C_{bi}) of bilirubin. The serum levels of the bilirubin were chosen as: 0, 5, 10, 15, 20 and 25 mg/dL while f_{bl} and f_{me} were held constant at 0.002 and 0.020, respectively.

The second simulation investigated the influence of the epidermal melanin pigment on the diffuse reflectance spectrum of a typical jaundice neonate (C_{bi} = 10 mg/dL = 0.10 g/L) with blood content f_{bl} = 0.002. Here the content of melanin was changed according to the values of f_{me} = 0 (amelanotic skin), 0.02 and 0.04 (lightly pigmented skin).

The third simulation was dedicated to the analysis of the dependence of the spectral diffuse reflectance with the blood content f_{bl}. The values of volume fraction of blood f_{bl} were chosen as: 0.001, 0.002, 0.01 and 0.02 while f_{me} and C_{bi} were held constant at 0.02 and 10 mg/dL, respectively. The maturity of the skin was assumed to be 39 weeks which specified the dermal scattering properties of neonatal skin. Hemoglobin concentration of 150 g/L, oxygen saturation S = 0.70 and a refractive index of 1.5 for neonatal skull, respectively, were assumed in all simulations above.

The fourth and fifth simulations were performed to investigate how variations in the refractive index of skull and fatty tissue would affect the diffuse reflectance spectrum of skin, respectively. There is not abundant literature about the refractive index of neonatal skull (Gibson et al., 2001). Therefore, we assumed that this bone has a refractive index similar to the refractive index reported in published literature concerning techniques for dissection and measurement of refractive index of osteones with different grade of mineralization (Ascenzi & Fabry, 1959). To study the effect of skull refractive index on reflectance spectrum we assumed this parameter to vary in the range 1.5-1.56 with an increment of 0.02. On the other hand to investigate the influence subcutaneous tissue refractive index on reflectance spectra this parameter was varied in the range 1.44-1.50 with an increment of 0.02.

3. Results and discussions

The total absorption coefficient of dermis for the first and third simulation described in subsection 2.3 is plotted in figure 2 following equations of subsection 2.2. In figure 3 is shown the total absorption coefficient of epidermis according to specifications of the second simulation.

In figure 2 A) are shown the resulting absorption spectra of dermis at different bilirubin concentrations. It is observed, as expected according to equations (2) and (3) that the total absorption coefficient of dermis is linearly increased with bilirubin concentration, C_{bi}. In addition, the absorption profile goes comparatively from a narrow curve for the lowest

concentration (C_{bi} = 0, only blood is absorbing) to a wide spectral shape for the highest bilirubin concentration (C_{bi} = 0.25 g/L) which corresponds to an extremely dangerous physiological concentration. In figure 2 B) are shown the resulting absorption spectra of dermis at different values of the blood volume fraction. It is observed, as expected according to equations (3), (4) and (5) that the total absorption coefficient of dermis is linearly increased with blood content, f_{bl}. The monotonically decreasing behavior of total absorption coefficient of epidermis is depicted in figure 3 and is a direct consequence of the analytical expression for the absorption coefficient of the interior of a melanosome (Jacques, 1998) and equation (1).

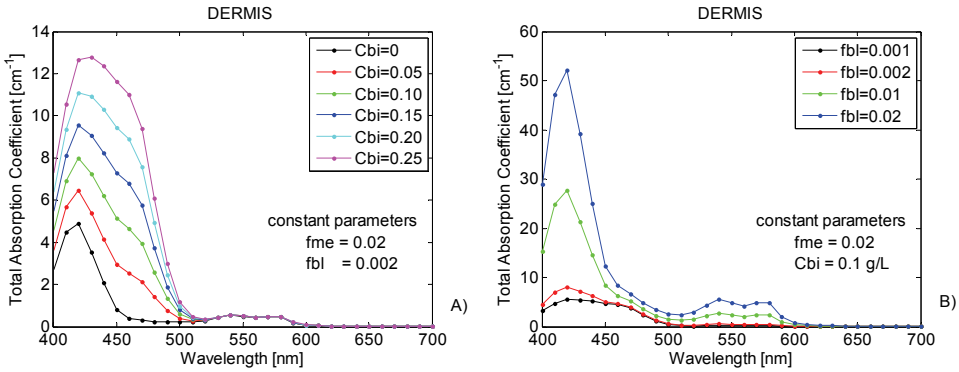

Fig. 2. Absorption coefficient of dermis for the optical model presented in subsection 2.2. A) The bilirubin concentration in the blood, C_{bi}, is varied. B) The volume fraction of blood vessels, f_{bl},is varied.

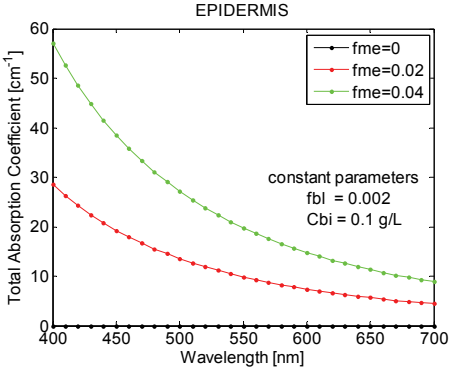

Fig. 3. Absorption coefficient of epidermis for the optical model as the volume fraction of melanosomes, f_{me}, is varied.

In figure 4 A) is shown diffuse reflectance spectra for several bilirubin concentrations. It is observed that the spectra change their shape in the range of 400-520 nm with the amount of added bilirubin. It is also important to note the non- linear relationship between bilirubin concentration and diffuse reflectance in the 400-520 nm spectral region. The decrease in diffuse reflectance with added bilirubin is not proportional to bilirubin, which is an

important factor during the development of algorithms to assess the bilirubin concentration *in-vivo* in jaundiced neonates.

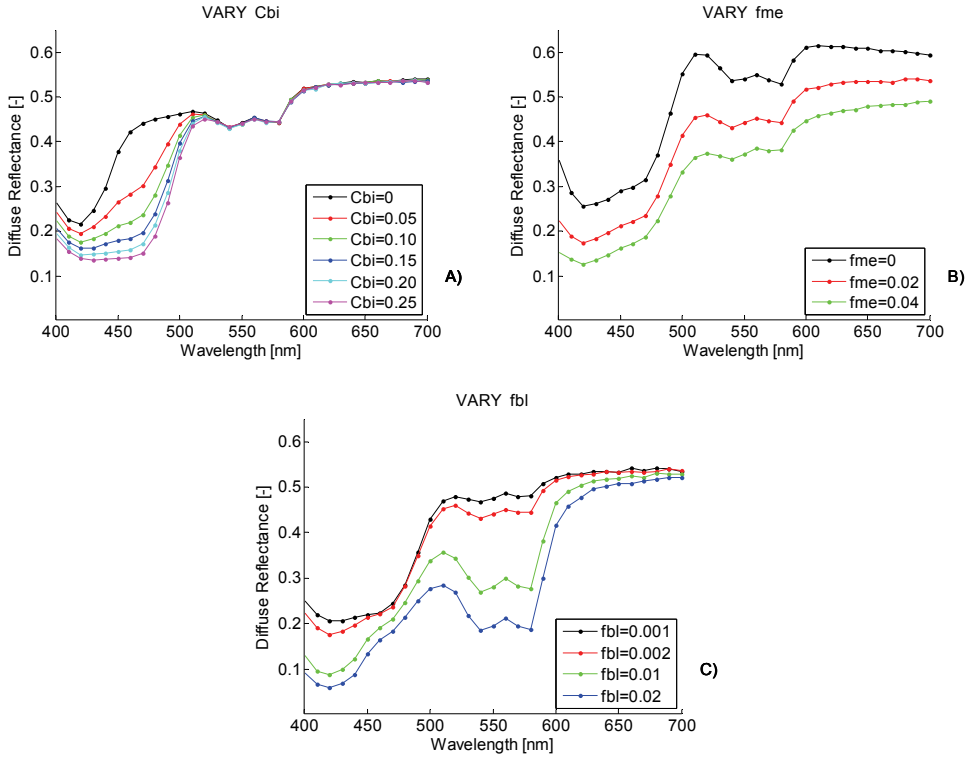

Fig. 4. Diffuse reflectance spectra that result from the Monte Carlo simulation for the three simulated situations. A) First simulation: bilirubin concentration is varied. B) second simulation: volume fraction of melanosomes is varied. C) Third simulation: blood vessels volume fraction is varied.

Figure 4 B) shows the diffuse reflectance spectra when the epidermal melanin pigmentation is varied. In this case, for the same concentration of bilirubin (10 mg/dL, representing a typical jaundiced neonate) a remarkable change in the diffuse reflectance occurs across the whole spectral range (400 to 700nm).

It is important to take into account this result when designing and developing the devices and methods to determine bilirubin levels based on spectroscopic, imaging or color techniques because they mainly record and process the spectral diffuse reflectance.

We consider that in order to make a more complete study further simulations are required to evaluate the dependence of this result for volume fraction of melanosomes that are representative of neonates with moderately and darkly pigmented skin.

In figure 4 C) is shown reflectance spectrum of skin when the content of blood f_{bl} is varied. For a relatively small change of this parameter (from 0.002 to 0.001) the most notable influence on diffuse reflectance is located near the following central wavelengths: 420, 542 and 578 nm. It is important to note that for the ranges 450-500 nm and 600-700 nm the

reflectance practically do not change with this small change in blood. However, when a relatively greater change of f_{bl} is used, for instance from 0.002 to 0.01 or 0.02, a considerable change occurs in the reflectance spectrum for the 450-500 nm spectral region and in general in the whole spectral region 400-650 nm. It is observed from this figure that the impact of blood on Rd(λ) is minimal in the 650-700 nm range (red light). A tendency to minimal change of reflectance for near infrared wavelengths is expected. So in a future work MC simulations should be performed considering an extension of the visible spectral region used in this work.

It is easy to see the so called characteristic ''W'' pattern (Angelopoulou, 1999) that appears within the 500-600 nm range and the pronounced valley at 420 nm for the larger values of f_{bl} (0.01 or 0.02). This result expresses the importance of considering the individual variability of blood content during the assessment of transcutaneous bilirubin levels by optical methods. The simulation reproduces qualitatively the results reported by Jacques using diffusion theory to simulate reflectance spectrum of jaundiced newborns (Jacques et al., 1997).

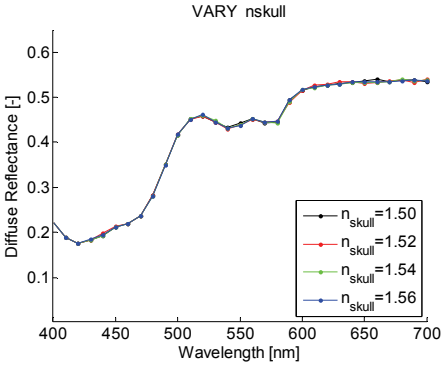

Fig. 5. Diffuse reflectance spectra of neonatal skin when the refractive index of skull is varied while the remaining parameters (C_{bi} = 0.1 g/L, f_{bl} = 0.002, f_{me} = 0.02 and n_{fat} = 1.44) of the model are kept constant.

In figure 5 is shown the reflectance spectra when the refractive index of skull is varied. As can be observed from this figure the variation of skull refractive index, n_{skull}, in a realistic range (1.50-1.56) does not affect the diffuse reflectance spectrum for the three-layer model presented in this study. From the individuality of the growing and expansion processes of brain and skull in neonates it could be expected that at birth differences of mineralization and ossification could be present and hence the refractive index of skull might change accordingly to these processes. The significance of the result summarized in figure 5 is precisely that attention should not be paid to individual variation of skull refractive index when the diffuse reflectance is measured in the visible spectral range. Therefore, a correction factor is not necessary to be included in the algorithm of determination of transcutaneous bilirubin level to account for the different grade of maturity of neonate's skull. This picture dramatically changes when the fat refractive index of subcutaneous tissue (fatty tissue) is changed in this model as we will comment in next paragraph.

Figure 6 illustrates the reflectance spectra for various refractive indexes of subcutaneous layer, n_{fat} . For $\lambda < 500$ nm there is a null difference among reflectance spectra whereas for wavelengths in the region 500 nm $<\lambda <$ 600 nm there is a slight increase of the difference among reflectance spectra. The spread of reflectance spectra is maximal for λ>600 nm where

maximum difference between spectrum for n_{fat} =1.44 and the spectrum for n_{fat} =1.54 is about 4% with respect to the average spectral curve. A closer view of this spectral region reveals that there is a trend of reflectance spectrum to diminish as the fat refractive index, n_{fat}, is increased.

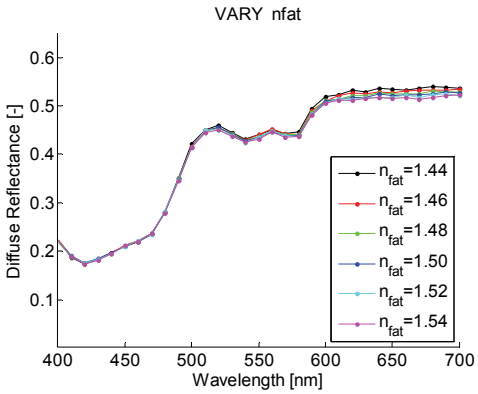

Fig. 6. Diffuse reflectance spectra of neonatal skin for various refractive index of subcutaneous tissue while the remaining parameters (C_{bi} = 0.1 g/L, f_{bl} = 0.002, f_{me} = 0.02 and n_{skull} = 1.50) of the model are kept constant.

One important and general observation is done here. If we turn reflectance spectra into optical density OD or absorption spectra A:

$$A(\lambda) = -\log_{10} R(\lambda) \tag{8}$$

a linear analysis can be used to interpret A(λ) in terms of the melanin, blood and bilirubin concentrations. On the other hand, a relatively simple inversion algorithm could be implemented based on the combination of the main results presented in figure 4 (section 3) with a diffusion approximation theory for light transport in tissue to solve the inversion problem. The basic ideas of this problem are briefly discussed in next section and detailed information will appear in a forthcoming research work.

4. Inverse problem

So far we have just analyzed the direct problem, that is how physiological parameters: bilirubin concentration, Cbi; blood content, fbl; melanin pigmentation content, fme; and refractive indexes of skull, and fat layer, respectively affect the simulated diffuse reflectance spectrum of a given optical model for neonatal skin. However, what is more important for practical purposes is to solve the inverse problem: determining bilirubin levels in jaundiced newborns from spectra despite the variation of melanin and blood. Especially it is encouraging not to use the whole spectra to solve this problem but rather to use few reflectance values at specific wavelengths. That is precisely what will be presented in the next paragraphs.

4.1 Principles of the inverse algorithm

The inverse algorithm is based on the use of an approximate diffusion theory expression for the total diffuse reflectance:

$$R_d(\lambda) = \exp(-\mu_a(\lambda)8d(\lambda)) \quad (9)$$

where $d = \sqrt{D/\mu_a}$ and $D = 1/(3(\mu_a + \mu_s'))$ are the optical depth penetration coefficient and the diffusion coefficient, respectively. These coefficients are in turn calculated from the basic optical parameters of the tissue which are wavelength dependent as it is well known.
The main steps of the algorithm are briefly outlined:

Step 1. {Cbi, fbl, fme}
Generate the dependence $R_{700}=F_1(fme)$ and using the inverse function $fme= F_1^{-1}(R_{700})$ determine the melanin content fme from a "measurement" of diffuse reflectance for the wavelength of 700 nm (R_{700}). Hence, the main output of this step is the extracted value of melanin content, fme_ext.

Step 2. {Cbi, fbl, fme_ext}
Generate the dependence $R_{578} =F_2(fbl)$ and using the inverse function $fbl=F_2^{-1}(R_{578})$ determine the blood content fbl from a "measurement" of diffuse reflectance for the wavelength of 578 nm (R_{578}). Therefore, the principal output of this step is the extracted value of blood content, fbl_ext.

Step 3. {Cbi, fbl_ext, fme_ext}
Generate the dependence $R_{460} =F_3(Cbi)$ and using the inverse function $Cbi=F_3^{-1}(R_{460})$ determine bilirubin concentration Cbi from a "measurement" of diffuse reflectance for the wavelength of 460 nm (R_{460}). So, the principal goal of this step is the extracted value of bilirubin content, Cbi_ext.

The above steps were programmed in matlab programming language and saved into a code called Inverse_MAIN.m which contains several subroutines to perform the steps described above. The program yields the extracted values: fme_ext, fbl_ext, and Cbi_ext from a test spectrum of known physiological parameters fme_true, fbl_true and Cbi_true.

4.2 Case study

In this section we test the accuracy of the recovery of Cbi parameter as function of the grade of hyperbilirubinemia. In order to do this, we consider a set of spectra corresponding to known serum levels of bilirubin (Cbi_true) chosen as: {0.015, 0.045, 0.075, 0.105 g/L} and {0.155, 0.205, 0.255 g/L} to include jaundice cases classified as hyperbilirumemia and excesive hyperbiliruminemia, respectively. These spectra were synthesized corresponding to a population of high melanin pigmentation fme = 0.20 (20%) following the criterion that appears in published literature (Jacques, 1998). The blood content, fbl was held constant at 0.002 (0.2%) which corresponds to a typical value of this parameter for human skin. Therefore, seven synthetic spectra were generated and saved for the above described physiological parameters. The use of synthetic spectra for which true physiological parameter (Cbi, fbl, fme) values are known allows quantitative estimation of the recovery accuracy of the algorithm proposed. The figure of merit to quantify this accuracy is the recovery relative error, which is calculated as the ratio of the difference between the extracted and true parameter to the true parameter, (extracted – true)/true. This recovery error is expressed in percentage.
The spectra as defined above were loaded into the inverse Matlab algorithm (Inverse_MAIN.m) in order to perform the extraction of bilirubin concentration (Cbi_extracted). The results of extracted values are shown in figure 7. From figure 7 A) it is qualitatively observed that, our algorithm retrieves the bilirubin content, Cbi, correctly which is based on the proximity between the obtained result and the expected ideal result plotted values. This is quantitatively represented in figure 7 B) where the extraction error of

Cbi is showed as function of true Cbi values. From this last figure is concluded that with bilirubin content, Cbi, in the range 0.045-0.255 g/L the extraction error of our recovery algorithm is less than 6%.

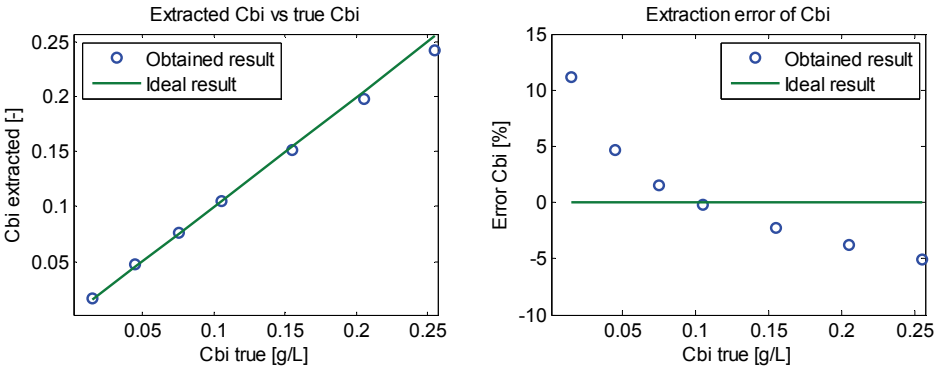

Fig. 7. Result of the inverse algorithm for the case study presented in subsection 4.2 A) Cbi extracted value vs Cbi true value. B) Extraction error vs true Cbi value.

5. Concluding remarks

The Monte Carlo code (MCML) used in this chapter in combination with the simplified optical model proposed for neonatal skin predicts the behavior of reflectance spectra of a jaundiced skin when bilirubin, melanin and blood content are variable physiological parameters. Regarding this fact three direct conclusions are drawn as follows: First, the effect of melanin (homogeneosly distributed in a 40 μm epidermis layer) on Rd(λ) is strong in the 650-700 nm range (red light), while blood and bilirubin have no effect. Therefore, the deep red wavelength range can specify the epidermal melanin content. Second, the impact of blood on Rd(λ) is maximal in the 540-580 nm range (green/yellow/orange light), while bilirubin has no effect in this spectral region. Hence the yellow wavelength range, after correcting for melanin, can specify the dermal blood content. Third, the influence of bilirubin on Rd(λ) is maximum around 460 nm (blue light). So the blue wavelength range, after correcting for melanin and blood, can specify the bilirubin content of dermal skin.

On the other hand the simulation results suggest that there is a wide range over which the refractive index of neonatal skull has a null effect on the reflectance curves whereas a more significant influence on reflectance spectra was observed when the fat refractive of the subcutaneous layer was allowed to change.

The practical significance of the above conclusions is that a simple low-cost hand-held bilirubin meter can be built with three LEDs (red, yellow and blue light-emitting diodes), to specify bilirubin levels despite variations in the melanin or blood content of a newborn's skin. Such a device would have a tremendous impact on the world-wide health of newborns, with minimal cost. This last idea is reinforced in this study by a preliminary implementation of an inverse algorithm to recover the bilirubin concentration, Cbi, from discrete measurement of diffuse reflectance at specific wavelengths in the visible spectrum, namely 460 nm, 578 nm and 700 nm.

The combination of Matlab codes presented in this chapter (MCinput.m and MCoutput.m) and MCML Monte Carlo code can serve as a valuable tool for the spectral simulation of

other physical quantities within the output data file generated by the MCML code. To do this only a precise knowledge of the structure this file and slight modifications of Matlab codes are required. In order to make more realistic simulations the work presented in this chapter should be improved by considering the extent and geometry of real LEDs beams, the emission-detection geometry and spectral feature of LEDs and detector, among other parameters.

Finally to conclude, some issues relating to the simulation are noted here. The direct Monte Carlo simulation of diffuse reflectance in neonatal skin is based on the use of spectral libraries of tabulated molar extinction coefficient for hemoglobin in water and bilirubin dissolved in chloroform, respectively (Prahl, accessed September 2010) but neither haemoglobin nor bilirubin in human skin are exactly dissolved in these conditions. Therefore a more realistic molar extinction coefficient should be determined to improve the reliability of future simulations. A fixed partition coefficient f_{bi} (kept constant at 0.20) was considered when, in reality, it should vary nonlinearly as C_{bi} exceeds holding capacity of serum albumin. This issue should be investigated in more detail to be included properly in next simulations. The recovery algorithm was based on the use of diffusion theory and in future work we will explored the possibility of an easy implementation of this algorithm using MC simulations to reformulate the three step method described in this chapter.

Appendix 1 Matlab codes MCinput.m and MCoutput.m

A) The code MCinput.m

```
%%%%%%%%%%%%%%%%%%%%%%%%%%%%%%%%%%%%%%%%%%%%%%%%
% MCinput.m is a matlab script
% to generate several input data files with extension .mci
% when bilirubin content, Cbi, is varied as the vector below:
% CBi = [0 0.05 0.1 0.15 0.20 0.25]
%%%%%%%%%%%%%%%%%%%%%%%%%%%%%%%%%%%%%%%%%%%%%%%%
% by J.A.Delgado Atencio
% Instituto Nacional de Astrofísica Óptica y Electrónica (INAOE), Puebla, México
% September 3, 2010
%%%%%%%%%%%%%%%%%%%%%%%%%%%%%%%%%%%%%%%%%%%%%%%%
clear all
for l=1:6
CBi = [0 0.05 0.1 0.15 0.20 0.25]; CBi=CBi(l);          % Bilirubin content in [g/L]
H1='C:\INTECH Book_2010\WORKSHOPS\'                      % files address
H2=sprintf('Cbi_%d-APPENDIX.mci',l); H=[H1 H2];          % Name of input data files
% 1 SIMULATION PARAMETERS-I  ---> The grid and number of photons
Nf=50000                                                 % No. of photons
dz=20E-4 , dr=20E-4                                      % dz, dr of the grid
Nz=62 , Nr=200 , Na=1                                    % No. of dz, dr & da.
% 1 SIMULATION PARAMETERS-II---> Geometrical and optical properties of layers
nc=3;                                                    % Number of layers
nabove=1.00;                                             % Refractive index TOP medium
n1=1.37,d1=40E-4;                                        % Layer 1 of 3
n2=1.37,d2=900E-4;                                       % Layer 2 of 3
n3=1.44,d3=300E-4;                                       % Layer 3 of 3
nbelow=1.5;                                              % Refractive index BOTTOM medium
fme=2/100;                                               % MELANIN content kept constant
```

```
fbl=0.2/100;                                % BLOOD   content kept constant
fbi=20/100;                                 % Partition number
S  =70/100;                                 % Oxygen saturation
Cbl  =150;                                  % Typical Hb concentration [g/L]
P_Mbl=64500;                                % Molecular weight of Hb [g/moles]
CM1=Cbl/P_Mbl;                              % Constant, see equation (5)
CM2=Cbl/P_Mbl;                              % Constant, see equation (5)
P_Mbi=585;                                  % Molecular weight of Bi in [g/moles]
CM3=CBi/P_Mbi;                              % Constant, see equation (2)
% 1 SIMULATION PARAMETERS-III---> Spectral data
lambdai=400;lambdaf=700,step=10;            % Spectral region and increment
numruns=((lambdaf-lambdai)/step)+1;         % Number of runs
lambda=lambdai:step:lambdaf;                % Discret wavelengths
format long
% 2 OPTICAL PROPERTIES
% ABSORPTION and SCATTERING in <<EPIDERMIS>>
miuame=(6.6*10^11)./(lambda.^3.33);         %Absorption coefficient of melanosome
mua1= fme*miuame;                           % Epidermis absorption coefficient
g=0.62 + (0.29E-3).*lambda;                 % Anisotropy factor
miuspN= 68*(1-(1.745*10^(-3)).*lambda + (9.8443*10^(-7)).*lambda.^2 ) +
(9.5*10^(11)).*(lambda.^(-4));
mus1=miuspN./(1-g);                         % Epidermis scattering coefficient
% ABSORPTION and SCATTERING  in <<DERMIS>>
kindexi=((lambdai-350)/2)+1;                % Measurement step= 2nm
kindexf=((lambdaf-350)/2)+1;
kindex=(kindexi:step/2:kindexf);
load MEHemoglobin.txt –ascii                % Load Hb extinction coefficient
MEHemoglobin;
ExtHbO2=MEHemoglobin(:,2);
ExtHb    =MEHemoglobin(:,3)
E1=ExtHbO2(kindex);
E2=ExtHb(kindex)
miuasangreHbO2=CM1*(log (10)).*E1;          % See equation (5)
miuasangreHb    =CM2*(log (10)).*E2;        % See equation (5)
mindexi=(lambdai-350)/(0.25)+1;             % Measurement step= 0.25nm
mindexf=(lambdaf-350)/(0.25)+1
mindex=(mindexi:step/0.25:mindexf);
load MEBilirubin.txt -ascii;                % Load bilirubin extinction coefficient
MEBilirubin;
ExtBi=MEBilirubin(:,2);
E3=ExtBi(mindex)
miuabilirubin=CM3*(log (10)).*E3;
mua2= fbl.*(S.*[miuasangreHbO2'] + (1-S).*[miuasangreHb'])+ fbi.*([miuabilirubin']);
color='krgbcm'; color=color(l);
% Verification of dermal absorption by plotting
plot(lambda,mua2,color);
hold on
mus2=miuspN./(1-g);
```

```
% ABSORPTION and SCATTERING in <<HYPODERMIS>>
mua3=1
mus3=600
g3=0.8
% 3 WRITE INPUT DATA FILES FOR EACH WAVELENGTH
fout= fopen(H,'wt');
fprintf(fout,'####\n');
fprintf(fout,'#  Template of input files for Monte Carlo simulation (mcml).\n');
fprintf(fout,'#  Anything in a line after "#" is ignored as comments.\n');
fprintf(fout,'#  Space lines are also ignored.\n');
fprintf(fout,'#  Lengths are in cm, mua and mus are in 1/cm.\n');
fprintf(fout,'####\n\n');
fprintf(fout,'1.0\t\t\t\t\t\t# file version\n');
fprintf(fout,'%1d\t\t\t\t\t\t# number of runs\n\n',numruns);
for k=1:numruns
fprintf(fout,'### Specify data for run %2d\n',k);
fprintf(fout,'%d.mco\t\tA\t\t\t\t# output filename, ASCII/Binary\n',lambda(k));
fprintf(fout,'%2d\t\t\t\t\t\t# No. of photons\n',Nf);
fprintf(fout,'%5.4f\t%5.4f\t\t\t\t\t# dz, dr\n',dz,dr);
fprintf(fout,'%1d\t%2d\t%2d\t\t\t\t# No. of dz, dr & da.\n\n',Nz,Nr,Na);
fprintf(fout,'%1d\t\t\t\t\t\t# No. of layers\n', nc);
fprintf(fout,'# n\tmua\tmus\tg\td\t\t# One line for each layer\n');
fprintf(fout,'%3.2f\t\t\t\t\t\t# n for medium above.\n',nabove);
fprintf(fout,'%3.2f\t%5.3f\t%5.3f\t%3.4f\t%5.4f\t\t# layer
1\n',n1,mua1(k),mus1(k),g(k),d1);
fprintf(fout,'%3.2f\t%5.3f\t%5.3f\t%3.4f\t%5.4f\t\t# layer
2\n',n2,mua2(k),mus2(k),g(k),d2);
fprintf(fout,'%3.2f\t%5.3f\t%5.3f\t%3.4f\t%5.4f\t\t# layer 2\n',n3,mua3,mus3,g3,d3)
fprintf(fout,'%3.2f\t\t\t\t\t\t# n for medium below.\n\n\n',nbelow);
end
fclose(fout)
end
```

B) The code MCoutput.m

```
%%%%%%%%%%%%%%%%%%%%%%%%%%%%%%%%%%%%%%%%%%%%%%%%%
% MCoutput.m is a matlab script
% to read diffuse reflectance from six folders (ncarp=6) called
% CBi_1 , CBi_2....CBi_6 where each of them contain 31 MC ouput files called
% 400.mco, 410.mco.......700.mco
% CBi = [0 0.05 0.1 0.15 0.20 0.25]
%%%%%%%%%%%%%%%%%%%%%%%%%%%%%%%%%%%%%%%%%%%%%%%%%
% by J.A. Delgado Atencio
% Instituto Nacional de Astrofísica Óptica y Electrónica (INAOE), Puebla, México
% September 3, 2010
%%%%%%%%%%%%%%%%%%%%%%%%%%%%%%%%%%%%%%%%%%%%%%%%%
clear all
name='Cbi';                                % Name of the folders to open
ncarp=6;                                   % Number of folders
```

```
for j=1:ncarp
  fname1=sprintf('Diffuse_reflectance_%d.txt',j);        % Name of saved spectra files
  address1='C:\INTECH Book_2010\WORKSHOPS\';
  namecarp= [name ,'_%d']; folder1=sprintf(namecarp,j); slasht1='\';
  total1= [address1 , folder1, slasht1, fname1];
  fid_w= fopen(total1, 'wt');                            % Open file .txt to write spectrum
  for k=400:10:700
  fname=sprintf('%d.mco',k);
  total = [address1, folder1, slasht1, fname];
  fid_r= fopen(total, 'rt');                             % Open file .mco to read reflectance
  for i=1:13
    line = fgetl(fid_r);                                 % Get the name of output file .mco
    end
    name1    = sscanf(line,'%sc');
    bindex=(1:1:3);
    I=double(name1);
    m=I(bindex);
    s=char(m);
    lambda=str2num(s);
    for i=14:28
    line = fgetl(fid_r);                                 % Get the reflectance from file .mco
    end
    Rd    = sscanf(line,'%f');
    fprintf(fid_w,'%f\t',lambda);                        % Write wavelength and the reflectance
    fprintf(fid_w,'%f\n',Rd);                            % to the opened file .txt
    fclose(fid_r);                                       % Close file .mco
  end
 fclose(fid_w);                                          %Close file .txt
end
% Plotting  comparative spectra to reproduce figure 4 A) of this chapter
format long
for m=1:ncarp
  fname3=sprintf('Diffuse_reflectance_%d.txt',m);
  folder3=sprintf(namecarp,m);
  total3= [address1, folder3, slasht1, fname3];
  fid3 = fopen(total3 ,'rt');
  B  = fscanf(fid3, '%f %f', [2 inf]);
  B  = B';
  fclose(fid3);
     hold
  X1=B(:,1);                                             % Wavelength [nm]
  Y1=B(:,2);                                             % Diffuse reflectance [-]
  figure(1)
  C1='krgbcm'; C1=C1(m);
  C2='.....'; C2=C2(m);
  C3='------'; C3=C3(m); C=[C1,C2,C3];
  plot(X1,Y1,C)
  sz=14;
```

```
 set(gca,'fontsize',sz)
 axis([400 700 0.003 0.65]);
 xlabel('Wavelength [nm]');
 ylabel('Diffuse Reflectance [-]');
 state='VARY  '; superior= [state , name];
 label1=sprintf(superior,j);
 title (label1)
 legend('Cbi=0','Cbi=0.05','Cbi=0.10','Cbi=0.15','Cbi=0.20','Cbi=0.25',4);
hold
end
```

5. Acknowledgment

The authors of this work would like to thanks to INAOE and CONACYT, México for the support for the development of this research work.

6. References

Metropolis, N. (1987). "The Beginning of the Monte Carlo Method." Los Alamos Science. Especial Edition, 125-130.

Weisstein, E.W. "Buffon's Needle Problem." from MathWorld A Wolfram Web Resource. http://mathworld.wolfram.com/BuffonsNeedleProblem.html, accessed April 5, 2007.

Danielson, R.E., Moore, D.R., van de Hulst, H.C. (1969). "The Transfer of Visible Radiation Through Clouds." Journal of the Atmospheric Science. Vol.10, No 6, 1078-1087.

Marchuk, G.I. et al, "The Monte Carlo Methods in Atmospheric Optics". English edition © Springer-Verlag Berlin Heidelberg 1980. Original Russian Edition 1974.

Wilson, B.C. & Adam, G. (1983). "A Monte Carlo Model for the absorption and flux distributions of light in tissues." Medical Physics. Vol.10, No 6, 824-830.

Hasegawa, Y., Yamada, Y., Tamura, M., Nomura, Y. (1991). "Monte Carlo simulation of light transmission through living tissues." Appl. Optic. Vol. 30, Issue 31, pp. 4515-4520.

Graaff, R., Koelink, M.H., de Mu1, F.F.M., Zijlstra, W.G., Dassel, A.C.M and Aamoudse, L.G. (1993) "Condensed Monte Carlo simulations for the description of light transport" Appl. Opt. Vol. 32, pp. 426-434.

Wang, L., Jacques, S.L, Zheng L. (1995). "MCML-Monte Carlo modeling of light transport in multi-layered tissues". Computers Methods and Programs in Biomedicine 47, 131-146.

Wang, L., Jacques, S.L., Zheng L. (1997). "CONV-Convolution for responses to a finite diameter photon beam incident on multi-layered tissues". Computers Methods and Programs in Biomedicine 54, 141-150.

Alerstam, E., Svensson, T., Andersson-Engels, S. (2008). "Parallel computing with graphics processing units for high-speed Monte Carlo simulation of photon migration." J Biomed Opt; 13(6):060504.

Lo, W., Redmond, K., Luu, J., Chow, P., Rose, J., Lilge. (2009). "Hardware acceleration of a Monte Carlo simulation for photodynamic therapy treatment planning." Journal of Biomedical Optics, vol. 14, p. 014019.

Bhutani, V. K., Gourley, G.R., Adler, S., Kreamer, Bill., Dalin, Chris., Johnson, L.H. (2000). "Noninvasive measurement of total serum bilirubin in a multiracial predischarge newborn population to assess the risk of severe hyperbilirubinemia" Pediatrics Vol. 106 No. 2, 1-9.

Groenendaal, F., van der Grond, J., de Vries, L.S. (2004). "Cerebral metabolism in severe neonatal hyperbilirubinemia" Pediatrics Vol. 114 No. 1, 291-294.

Maisels, M.J et al. (Subcommittee on hyperbilirubinemia), (2004). "Management of hyperbilirubinemia in the newborn infant 35 or more weeks of gestation " Pediatrics Vol. 114; 297-316.

Rubaltelli, F.F., Gourley, G.R., Loskamp, N., et al. (2001). "Transcutaneous bilirubi measurement: a multicenter evaluation of a new device". Pediatrics. Vol. 107:1264–1271.

Maisels, M.J., Ostrea, E.J., Touch, S., et al. (2004). "Evaluation of a new transcutaneous bilirubinometer". Pediatrics. Vol. 113:1638–1645.

Jacques, S.L., Saidi, I., Ladner., A., Oelberg, D. (1997). "Developing an optical fiber reflectance spectrometer to monitor bilirubinemia in neonates". SPIE Proceedings 2975:115-124, Laser-Tissue Interactions, San Jose, CA Feb.

Delcher, H.K., Newman, G., Bambot, S., Jacques, S.L. "Transcutaneous bilirubin measurement in a mixed population: clinical evaluation of a new device." http:// www.spectrx.com/techdata/bilirubin/paperweb.pdf ., accessed April 5, 2007.

Kolman, K.B., Mathieson, K.M., Frias, C. (2007) "A Comparison of transcutaneous and total serum bilirubin in newborn hispanic infants at 35 or more weeks of gestation"

Wang, L., & Jacques, S.L. (Copyright © 1992 - 1998). "Monte carlo modeling of light transport in multi-layered tissues in standard C", http://omlc.ogi.edu/pubs/ pdf/man_mcml.pdf.

Jacques, S.L. (1998). "Skin optics", http://omlc.ogi.edu/news/jan98/skinoptics.html. accessed January 5, 2006.

Prahl, S.A. "Tabulated molar extinction coefficient for hemoglobin in water", http:// omlc.ogi.edu/spectra/hemoglobin/summary.html. Accessed September 19, 2010.

Prahl, S.A. "Tabulated molar extinction coefficient for bilirubin dissolved in chloroform", http:// omlc.ogi.edu / spectra / PhotochemCAD / html / bilirubin.html. Accessed September 19, 2010.

van Gemert M.J.C., Jacques, S.L., , Sterenborg, H.J.C.M., Start, W.M. (1989). "Skin Optics" IEEE Transaction on biomedical engineering, Vol. 36. No.12.

Tsumura, N., Kawabuchi, M., Haneishi, H., Miyake, Y. "Mapping pigmentation in human skin by multivisible-spectral imaging by inverse optical scattering technique" http://www.mi.tj.chiba-u.jp/~tsumura/Tsumura/papers/CIC8_oxygen.pdf, accessed January 5, 2006.

Randeberg, L.N. (2005) "Diagnostic applications of diffuse reflectance spectroscopy". Doctoral thesis, Norwegian University of Science and Technology, Trondheim, June 2005, ISBN 82-471-7077-9

Ascenzi, A. & Fabry, C.(1959),"Technique for Dissection and Measurement of Refractive Index of Osteones" http://www.ncbi.nlm.nih.gov/pmc/articles/PMC2229768/ pdf/139.pdf, Accessed September 19, 2010.

Gibson, A., Yusof, R.M., Dehghani, H., Riley, J., Everdell, N., Richards, R., Hebden, J. C., Schweiger, M., Arridge, S.R. and Delpy, D.T. (2003)"Optical tomography of a realistic neonatal head phantom". Applied Optics, Vol. 42, No. 16, 3100-2116.

Angelopoulou, E. (1999) "The Reflectance Spectrum of Human Skin". Technical Report MS-CIS-99-29.http://repository.upenn.edu/cgi/viewcontent.cgi?article=1616& context =cis_reports. Accessed September 27, 2010.

Applications of Monte Carlo Methods in Biology, Medicine and Other Fields of Science

Edited by Prof. Charles J. Mode

ISBN 978-953-307-427-6
Hard cover, 424 pages
Publisher InTech
Published online 28, February, 2011
Published in print edition February, 2011

This volume is an eclectic mix of applications of Monte Carlo methods in many fields of research should not be surprising, because of the ubiquitous use of these methods in many fields of human endeavor. In an attempt to focus attention on a manageable set of applications, the main thrust of this book is to emphasize applications of Monte Carlo simulation methods in biology and medicine.

InTech Europe
University Campus STeP Ri
Slavka Krautzeka 83/A
51000 Rijeka, Croatia
Phone: +385 (51) 770 447
Fax: +385 (51) 686 166
www.intechopen.com

InTech China
Unit 405, Office Block, Hotel Equatorial Shanghai
No.65, Yan An Road (West), Shanghai, 200040, China
中国上海市延安西路65号上海国际贵都大饭店办公楼405单元
Phone: +86-21-62489820
Fax: +86-21-62489821